Derivative moments in stationary homogeneous shear turbulence

By JÖRG SCHUMACHER

Department of Mechanical Engineering, Yale University, New Haven, CT 06520-8284, USA
and Fachbereich Physik, Philipps-Universität, D-35032 Marburg, Germany

A statistically stationary and nearly homogeneous turbulent shear flow is established by an additional volume forcing in combination with stress-free boundary conditions in the shear direction. Both turbulent energy and enstrophy are stationary to a much better approximation than in previous simulations that use remeshing. The temporal fluctuations decrease with increasing Reynolds number. Energy spectra and shear-stress cospectra show that local isotropy is satisfactorily obeyed at the level of second-order moments. However, derivative moments of high order up to $n = 7$ yield increasing moments for $n \geqslant 4$ for the spanwise vorticity and the transverse derivative of the streamwise velocity in the range of Taylor Reynolds numbers $59 \leqslant R_\lambda \leqslant 99$. These findings, which are in apparent violation of local isotropy, agree with recent measurements.

1. Introduction

Turbulent flows in nature and the laboratory are mostly anisotropic on their largest scales. A typical situation is one in which an imposed shear gradient sustains the turbulence. One fundamental question is the effect of anisotropic large scales on the statistical behaviour of the smaller scales. Kolmogorov (1941) postulated that at sufficiently large Reynolds number statistics of small scales become isotropic even if the large-scale driving is anisotropic. Consequently, cross-correlations, indicated e.g. by the shear-stress cospectrum $E_{xy}(k)$ in the Fourier space, should decay very fast to zero with respect to increasing wavenumber. Based on this postulate, Lumley (1967) predicted, for a turbulent shear flow with constant mean shear rate S, the rate at which anisotropy vanishes with decreasing scale size. If the shear time scale, $T_s = S^{-1}$, is much greater than the viscous time scale, $\tau_\eta = (\nu/\epsilon)^{1/2}$, in other words, if $S\tau_\eta \ll 1$ holds, he showed by dimensional arguments that the shear-stress cospectrum follows $E_{xy}(k) \sim \epsilon^{1/3} S k^{-7/3}$. Quantities ν and ϵ are the kinematic viscosity and the energy dissipation rate, respectively. Note that the cospectrum would be exactly zero in a system that is perfectly isotropic on all scales. The concept of local isotropy at the level of second-order moments seemed to be supported by direct numerical simulations (She *et al.* 1993) and a number of high-Reynolds-number measurements in turbulent boundary layers (Caughey, Wyngaard & Kaimal 1979; Saddoughi & Veeravalli 1994). Very recently, however, Kurien & Sreenivasan (2000) found a slower decay of anisotropies in an atmospheric boundary layer at $R_\lambda \approx 2000$. They reported, e.g. a scaling of the cospectrum with $E_{xy}(k_x) \sim k_x^{-2.1}$. Deviations from the local isotropy were also found in a number of new experiments in nearly homogeneous

shear flows when attention was focused on higher-order moments (Garg & Warhaft 1998; Ferchichi & Tavoularis 2000; Shen & Warhaft 2000).

Quantities which are very sensitive to anisotropic contributions at smallest scales are derivative moments of the turbulent velocity components, u_i'. We denote moments of odd orders ($k = 1, 2, 3$) by

$$S_{2k+1}(\partial u_i'/\partial x_j) = \frac{\langle (\partial u_i'/\partial x_j)^{2k+1} \rangle}{\langle (\partial u_i'/\partial x_j)^2 \rangle^{k+1/2}}, \qquad (1.1)$$

and of even orders ($k = 2, 3$) by

$$K_{2k}(\partial u_i'/\partial x_j) = \frac{\langle (\partial u_i'/\partial x_j)^{2k} \rangle}{\langle (\partial u_i'/\partial x_j)^2 \rangle^{k}}. \qquad (1.2)$$

The brackets $\langle \cdot \rangle$ denote the ensemble average and no tensor summations are applied for i and j. If the turbulence in the shear flow is locally isotropic odd moments of the transverse derivative ($i = x, j = y$) should decay as R_λ^{-1}. Shen & Warhaft (2000) measured a slower decay of the derivative skewness, $S_3(\partial u_x'/\partial y) \sim R_\lambda^{-0.5}$, with a value of 0.2 at $R_\lambda \sim 1000$. The fifth moment $S_5(\partial u_x'/\partial y)$ remained constant while $S_7(\partial u_x'/\partial y)$ even increased in the range of Taylor Reynolds numbers between 100 and 1000. These results were confirmed in part by similar experiments of Ferchichi & Tavoularis (2000). Third-order transverse derivative moments of both experiments also agreed with those found in homogeneous shear flow simulations at $R_\lambda \sim 100$ (Pumir 1996). All the results indicate that the influence of large-scale anisotropies on the statistics of the smallest scales does not decay as fast as predicted by dimensional arguments, and in some cases may not decay at all.

This paper addresses the numerical investigation of statistical properties in the simplest shear flow configuration, the homogeneous shear flow. The flow is characterized by the following mean profiles of the velocity components:

$$\langle u_x \rangle = Sy, \quad \langle u_y \rangle = \langle u_z \rangle = 0, \qquad (1.3)$$

where x is streamwise (or downstream), y shear (or wall-normal), and z spanwise directions, respectively. The velocity components can be decomposed into a mean fraction and a fluctuating turbulent part, $u_i = \langle u_i \rangle + u_i'$ for $i = x, y$ and z. Besides finite difference methods with shear periodic boundary conditions (Gerz, Schumann & Elgobashi 1989), pseudospectral methods in a fully periodic domain using a remeshing (Rogallo 1981; Rogers & Moin 1987; Pumir 1996; Gualtieri *et al.* 2000) have mostly been used to model a homogeneous shear flow. In this method, it was harder to reach a stationary turbulent state. An alternative method to overcome this problem was suggested by Schumacher & Eckhardt (2000). The method avoids the remeshing that needs to be applied for the increasingly skewed grid of Rogallo (1981) and that corresponds to a time-periodic driving of the flow. A statistically stationary state for long times can be maintained by using stress-free boundary conditions in the y-direction and an appropriate body force. Results for third and fourth order agreed with those of Rogers & Moin (1987) and of Pumir (1996). Derivative skewness was weakly decaying with respect to R_λ. This paper extends that analysis. We systematically investigate the temporal fluctuations of the energy and enstrophy around their mean values and compare them with the findings of Pumir (1996) and Gualtieri *et al.* (2000). We show that the level of fluctuations around the mean quantities is much smaller and reaches values that are observed in turbulence measurements. Energy as well as shear-stress cospectra are studied. Inspired by recent experiments we extend the

Run no.	1	2	3	4	5
Re_s	500	1000	1000	2000	2000
R_λ	59	79	87	95	99
L_x/L_y	2π	4π	2π	4π	2π
L_z/L_y	2π	2π	2π	2π	2π
N_x	256	256	256	256	256
N_y	65	129	65	129	65
N_z	256	128	256	128	256
$k_{max}\eta$	2.82	2.48	1.62	1.54	1.00
$\Delta y/\eta$	0.57	0.50	0.99	0.80	1.60
λ/η	17.8	18.9	19.8	20.2	20.7
L/η	36.4	63.3	58.4	80.5	77.5

TABLE 1. The runs presented with their parameters: shear Reynolds number Re_s; Taylor Reynolds number R_λ; aspect ratios L_x/L_y and L_z/L_y; numbers of grid points N_x, N_y and N_z; the spectral resolution criterion $k_{max}\eta$; and the ratios of grid spacing in the y-direction Δy, of Taylor microscale λ, and of integral length scale L to Kolmogorov length η.

analysis systematically to higher-order derivative moments ($n \leqslant 7$) in the range of Taylor Reynolds numbers accessible. Non-decreasing higher-order moments indicate that very rare small-scale events may exist. We shall also discuss the problem of statistical convergence of higher-order moments in detail.

2. Numerical model

With length scales measured in units of the gap width L_y, and time scales in units of S^{-1}, the dimensionless form of the equations for an incompressible Navier–Stokes fluid become

$$\frac{\partial \boldsymbol{u}}{\partial t} + (\boldsymbol{u} \cdot \nabla)\boldsymbol{u} = -\nabla p + \frac{1}{Re_s}\nabla^2 \boldsymbol{u} + \boldsymbol{f}, \quad \nabla \cdot \boldsymbol{u} = 0, \quad (2.1)$$

where $p(\boldsymbol{x}, t)$ is the pressure, $\boldsymbol{u}(\boldsymbol{x}, t)$ the velocity field. The shear Reynolds number is $Re_s = S L_y^2/\nu$. In the x- and z-directions periodic boundary conditions apply. In the other direction the flow domain is bounded by two parallel flat surfaces that are assumed to be impenetrable and stress-free,

$$u_y = \frac{\partial u_x}{\partial y} = \frac{\partial u_z}{\partial y} = 0 \quad \text{for} \quad y = 0, L_y. \quad (2.2)$$

As discussed in more detail in Schumacher & Eckhardt (2001), the free-slip boundary conditions allow efficient numerical simulations with Fourier modes for the velocity components. The equations are integrated by means of a pseudospectral technique using a 2/3-rule de-aliasing. Time integration was done by means of a fifth order Runge–Kutta scheme with adaptive time stepping (Hairer, Nørsett & Wanner 1993). In table 1 the computational parameters are summarized for all the runs presented. The aspect ratio L_x/L_z and the shear Reynolds number Re_s were varied. It is also clear that the spectral resolutions in x- and y-directions are different, causing maximum wavenumber components of $k_{x,max}(= k_{z,max}) = 2\pi N_x/(3L_x)$ and $k_{y,max} = 2\pi N_y/3$, respectively, after de-aliasing. As a criterion for sufficient spectral resolution $k_{max}\eta \geqslant 1$ is used (Pope 2000) with Kolmogorov length scale $\eta = (\nu^3/\epsilon)^{1/4}$ and $k_{max} = \sqrt{8}\pi N_x/(3L_x)$ for a uniform grid. For the present model with different grid spacing in the three dimensions, we therefore take $k_{max} = ((k_{x,max}^2 + k_{y,max}^2 + k_{z,max}^2)/3)^{1/2}$.
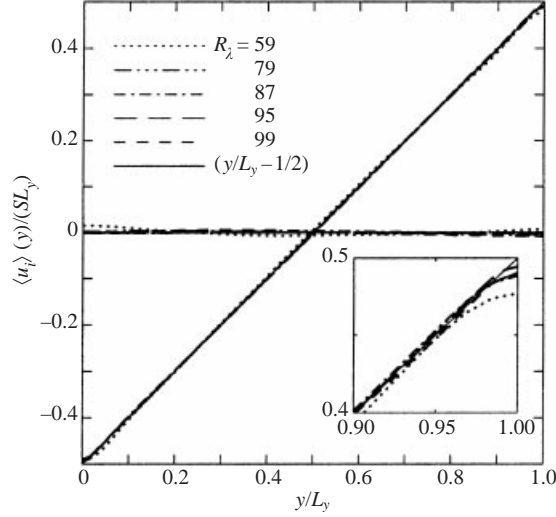
J. Schumacher

FIGURE 1. Mean velocity profiles of the three velocity components for different Reynolds numbers. The inset magnifies the profiles at the boundary $y/L_y = 1$ where deviations from transverse homogeneity are present. The thin solid line corresponds to the exact linear profile.

Additionally we plotted the ratio of grid spacing in the shear direction to the Kolmogorov scale, $\Delta y/\eta$, to indicate sufficient spectral resolution. The Taylor microscale λ is defined here with the downstream root-mean-square velocity

$$\lambda = \frac{\langle(u_x')^2\rangle^{1/2}}{\langle(\partial u_x'/\partial x)^2\rangle^{1/2}} = \frac{u_{x,rms}'}{(\partial u_x'/\partial x)_{rms}}, \tag{2.3}$$

and the integral length scale L is given by

$$L = \frac{1}{\langle(u_x')^2\rangle} \int_0^\infty dr \langle u_x'(x + re_x)u_x'(x)\rangle. \tag{2.4}$$

The Taylor Reynolds number follows as $R_\lambda = u_{x,rms}'\lambda/v$. The mean shear and turbulence are maintained by a suitable body force $f(x,t)$. An almost linear mean profile $\langle u_x\rangle(y) = (y - 1/2)$ for $y \in [0,1]$ (in dimensionless form) can be approximated by a finite Fourier sum of cosines

$$\langle u_x\rangle(y) \simeq -\frac{4}{\pi^2} \sum_{n=0}^{5} \frac{\cos[(2n+1)\pi y]}{(2n+1)^2}. \tag{2.5}$$

The external forcing f was chosen such that the six modes used in (2.5) remained constant in time, i.e. $\partial\text{Re}\{u_x(q,t)\}/\partial t = 0$ for Fourier modes with $q = (2n+1)\pi e_y$ for $n = 0$ to 5. It was shown by Schumacher & Eckhardt (2000) that this forcing, although itself varying with respect to time, causes the expected mean profiles of the velocity field components, $\langle u_y\rangle = \langle u_z\rangle = 0$ and $\langle u_x\rangle = y$ (see figure 1). The effects of the free-slip surfaces at $y = 0$ and $y = L_y$ on the bulk behaviour are much weaker than those of rigid walls, since only the wall-normal component is forced to vanish and a nearly homogeneous, statistically stationary turbulent state can be established.

Run no.	1	2	3	4	5
$\langle (u_x')^2 \rangle / q^2$	0.57	0.52	0.55	0.51	0.51
$\langle (u_y')^2 \rangle / q^2$	0.12	0.16	0.15	0.18	0.18
$\langle (u_z')^2 \rangle / q^2$	0.31	0.32	0.30	0.31	0.31
$-\langle u_x' u_y' \rangle / q^2$	0.11	0.12	0.11	0.12	0.12
S^*	7.32	8.18	8.58	8.22	8.37
$S\tau_\eta$	0.38	0.25	0.25	0.19	0.19
P/ϵ	1.04	1.00	0.99	1.01	1.01
$\tilde{\epsilon}$	1.18	0.87	0.70	0.77	0.72
$\sigma(\tilde{E})/\langle \tilde{E} \rangle_t$	0.20	0.12	0.11	0.09	0.10
$\sigma(\tilde{\Omega})/\langle \tilde{\Omega} \rangle_t$	0.23	0.13	0.12	0.09	0.10

TABLE 2. Physical properties of the homogeneous shear flow runs: the Reynolds stress components $\langle u_i' u_j' \rangle$, shear parameter S^*, the ratio of Kolomogorov time τ_η to shear time S^{-1}, the ratio of turbulence production to dissipation P/ϵ, and the dimensionless energy dissipation rate $\tilde{\epsilon}$. The last two rows list the ratio of standard deviation to the temporal mean for the specific turbulent kinetic energy, $\tilde{E} = E/(SL_y)^2$, and the enstrophy, $\tilde{\Omega} = \Omega/S^2$.
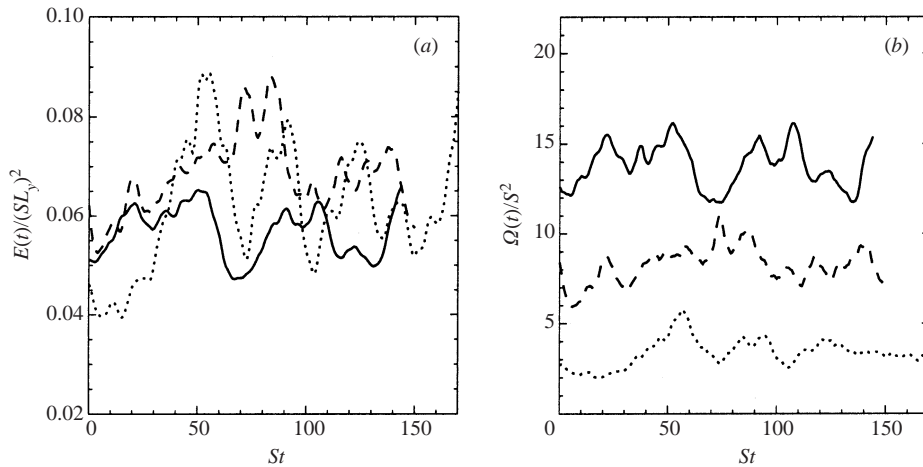

FIGURE 2. Temporal behaviour of (*a*) the specific turbulent kinetic energy $E(t)$ and (*b*) specific enstrophy $\Omega(t)$, for three values of Taylor Reynolds number: $R_\lambda = 59$ (dotted line), $R_\lambda = 87$ (dashed line), $R_\lambda = 99$ (solid line).

3. Energy balance and power spectra

Figure 2 shows the temporal evolution of the specific turbulent kinetic energy $E(t)$ and the specific enstrophy $\Omega(t)$ defined as

$$E(t) = \tfrac{1}{2}\langle (u_i')^2 \rangle_V, \quad \Omega(t) = \tfrac{1}{2}\langle (\omega_i)^2 \rangle_V, \qquad (3.1)$$

where $\langle \cdot \rangle_V$ denotes an average over the volume. The vorticity is defined as $\boldsymbol{\omega} = \nabla \times \boldsymbol{u}'$. The graphs indicate that a statistically stationary state is established in all cases. Additionally we analysed the ratio of the standard deviations $\sigma(E)$ and $\sigma(\Omega)$ to their corresponding temporal means, $\langle E \rangle_t$ and $\langle \Omega \rangle_t$. Both ratios were found to be smaller than for the results of remeshing simulations. Pumir (1996) and Gualtieri *et al.* (2000) reported ratios of about 50% for both energy and enstrophy at $R_\lambda \sim 90$. In contrast, we found a decrease of the ratios from about 23% at $R_\lambda = 59$ to 10% at $R_\lambda = 99$ (see table 2). The large fluctuations may thus be caused by the periodic driving due to the
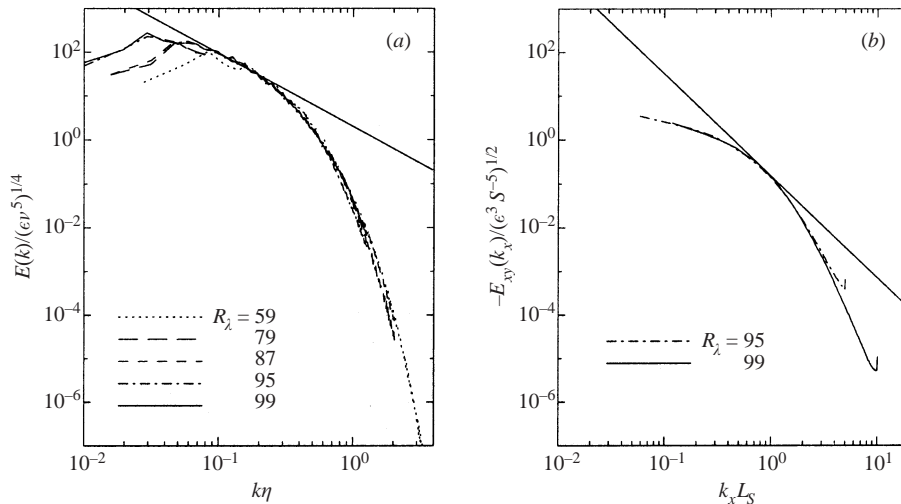
FIGURE 3. (*a*) Normalized energy spectra $E(k)/(\epsilon v^5)^{1/4}$ are plotted versus $k\eta$ for different values of R_λ. Straight solid line indicates scaling with $k^{-5/3}$ and $C_K = 2$. (*b*) Shear-stress cospectra $-E_{xy}(k_x)/(\epsilon^3 S^{-5})^{1/2}$ versus $k_x L_S$ with $L_S = (\epsilon S^{-3})^{1/2}$, for two values of R_λ. The straight solid line indicates scaling with $k_x^{-7/3}$ and $C_{xy} = 0.15$. Argument k_x was taken here in order to compare recent data to experimental findings.

remeshing, though this question still remains open. Statistical stationarity was further checked by comparing the ratio of turbulent production, $P = -\langle u'_x u'_y \rangle \partial \langle u_x \rangle / \partial y$, to the energy dissipation rate, $\epsilon = v \langle (\partial u'_i / \partial x_j)^2 \rangle$. The ratio P/ϵ was always found to be very close to 1 (see table 2). The shear parameter $S^* = Sq^2/\epsilon$ with $q^2 = \langle (u'_i)^2 \rangle$ remained nearly unchanged in the five simulations, consistent with a nearly constant ratio $-\langle u'_x u'_y \rangle / q^2$, which should equal $1/S^*$ in the stationary case.

Next we investigated the energy dissipation rate as a function of the Taylor Reynolds number. The expectation is that the energy dissipation rate at high Reynolds numbers is independent of viscosity, and is a constant of order unity when rescaled on the integral scale L and the root-mean-square velocity $u'_{x,rms}$, i.e. $\tilde{\epsilon} = \epsilon L/(u'_{x,rms})^3$. In table 2 the results are given for the present data: $\tilde{\epsilon}$ seems to saturate at order unity for R_λ between 80 and 100 which cannot be exceeded with the present grid resolution. A similar behaviour was found in the case of homogeneous isotropic turbulence (Sreenivasan 1998).

As also listed in table 2, about half of the total amount of velocity fluctuation is contained in the downstream component u'_x. The downstream fluctuations $\langle (u'_x)^2 \rangle (t)$ were found to always have a similar temporal shape to the total kinetic energies while the mean-square moments for both remaining components u'_y and u'_z have smaller variations with respect to time. We observed also that the fraction $\langle (u'_x)^2 \rangle / q^2$ with $q^2 = \langle (u'_i)^2 \rangle$ decreased slowly with respect to R_λ. Both aspects seem to be connected to the stronger fragmentation of coherent streaks and vortices (Schumacher & Eckhardt 2000, 2001) that is observed with increasing Re and the reduced downstream correlation of the velocity fluctuations.

In figure 3(*a*) we plot the kinetic energy spectra for five Taylor Reynolds numbers. With increasing values of R_λ a Kolmogorov scaling range can be observed for intermediate wavenumbers. The straight line is fitted with a (Kolmogorov) constant $C_K = 2$. It exceeds slightly the values of $C_K = 1.5$–1.6 known from high-Reynolds-number measurements (Pope 2000) which can be related to the bottleneck phenomenon

Run no.	1	2	3	4	5
$S_3(\omega_z)$	-7.9×10^{-1}	-7.1×10^{-1}	-6.7×10^{-1}	-6.9×10^{-1}	-6.3×10^{-1}
$K_4(\omega_z)$	5.6×10^0	6.4×10^0	6.6×10^0	6.6×10^0	7.3×10^0
$S_5(\omega_z)$	-8.9×10^0	-1.7×10^1	-1.7×10^1	-1.8×10^1	-1.9×10^1
$K_6(\omega_z)$	4.9×10^1	1.3×10^2	1.5×10^2	1.5×10^2	1.9×10^2
$S_7(\omega_z)$	-2.2×10^2	-7.4×10^2	-8.6×10^2	-8.8×10^2	-1.1×10^3
$S_3(\partial u'_x/\partial y)$	9.6×10^{-1}	9.2×10^{-1}	9.0×10^{-1}	9.2×10^{-1}	8.7×10^{-1}
$K_4(\partial u'_x/\partial y)$	5.6×10^0	6.4×10^0	6.4×10^0	7.2×10^0	7.1×10^0
$S_5(\partial u'_x/\partial y)$	1.0×10^1	2.0×10^1	2.0×10^1	2.5×10^1	2.1×10^1
$K_6(\partial u'_x/\partial y)$	5.0×10^1	1.3×10^2	1.3×10^2	2.0×10^2	1.7×10^2
$S_7(\partial u'_x/\partial y)$	2.1×10^2	7.4×10^2	7.5×10^2	1.4×10^3	9.5×10^2
$S_3(\partial u'_x/\partial x)$	-7.4×10^{-1}	-4.4×10^{-1}	-5.0×10^{-1}	-2.7×10^{-1}	-4.0×10^{-1}
$K_4(\partial u'_x/\partial x)$	6.3×10^0	4.8×10^0	5.3×10^0	4.3×10^0	5.0×10^0
$S_5(\partial u'_x/\partial x)$	-1.6×10^1	-6.9×10^0	-9.2×10^0	-3.7×10^0	-6.6×10^0
$K_6(\partial u'_x/\partial x)$	1.2×10^2	5.8×10^1	7.8×10^1	4.2×10^1	6.8×10^1
$S_7(\partial u'_x/\partial x)$	-6.1×10^2	-1.5×10^2	-2.6×10^2	-6.9×10^1	-1.7×10^2

TABLE 3. Derivative moments of order $n = 3, 4, 5, 6$ and 7 of the transverse derivative $\partial u'_x/\partial y$, the longitudinal derivative $\partial u'_x/\partial x$ and the spanwise vorticity ω_z.

(Falkovich 1994). This effect causes an energy pileup that can result in a larger C_K for the small scaling ranges observed here. In figure 3(*b*) the cospectra are compared. It is observed that their magnitude is always smaller by about two orders of magnitude than the kinetic energy spectrum over the whole range of wavenumbers, except the smallest. Both shear-stress cospectra fit the power law proposed by Lumley (1967) in a small range of wavenumbers. The constant C_{xy} was found here to be $C_{xy} \approx 0.15$, similar to the values found in high-Reynolds-number experiments (Saddoughi & Veeravalli 1994). As already mentioned, recent high-Reynolds-number measurements by Kurien & Sreenivasan (2000) indicated deviations from the $k_x^{-7/3}$ decay law. We note here that our Taylor Reynolds number is too small to draw any robust conclusion about the strength of deviations from the classical Kolmogorov–Lumley scaling, but the results do not seem to contradict the concept of local isotropy on the level of second-order moments.

4. Higher-order derivative moments

In this section, the quantities studied are those derivative moments that display sensitivity to deviations from local isotropy. Three different quantites were investigated: the transverse derivative of the turbulent streamwise velocity, $\partial u'_x/\partial y$, the spanwise vorticity, $\omega_z = \partial u'_y/\partial x - \partial u'_x/\partial y$, and the longitudinal derivative of the turbulent streamwise velocity, $\partial u'_x/\partial x$. In table 3 we summarize the results for orders 3 to 7 for five simulations. The moments of the longitudinal derivative $\partial u'_x/\partial x$ do not vary in order of magnitude for all values of n, and are found to agree with Ferchichi & Tavoularis (2000) as well as with Shen & Warhaft (2000). For a larger range of Taylor Reynolds numbers both experiments find a slow increase for all longitudinal moments. If the turbulent flow were isotropic, the odd moments $S_n(\partial u'_x/\partial y)$ would be exactly zero for all odd $n \geqslant 0$. In contrast, we observe non-zero values for the transverse derivative and spanwise vorticity moments. While the third order slowly decreases in the range of Taylor Reynolds numbers, fifth and seventh order increase with R_λ. In figure 4 we compare our results with the numerical data of Pumir
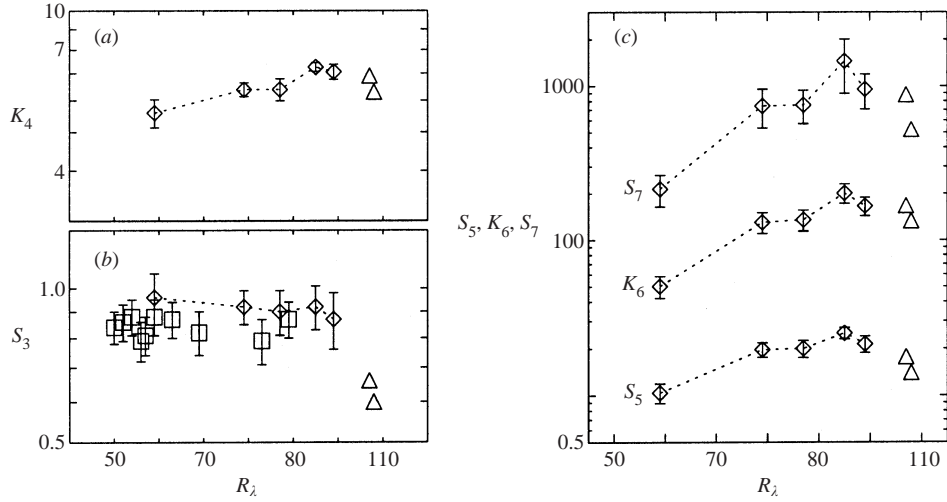
FIGURE 4. Higher-order moments of the transverse derivative $\partial u'_x/\partial y$ are compared with other numerical and experimental findings: (*a*) flatness K_4, (*b*) skewness S_3, (*c*) hyperskewness S_5, hyperflatness K_6 and the 7th moment S_7. $\square$, Pumir (1996); $\triangle$, Shen & Warhaft (2000); $\diamond$, present data. Error bars for $\diamond$ are calculated with respect to the variation of the data points in the *y*-direction.
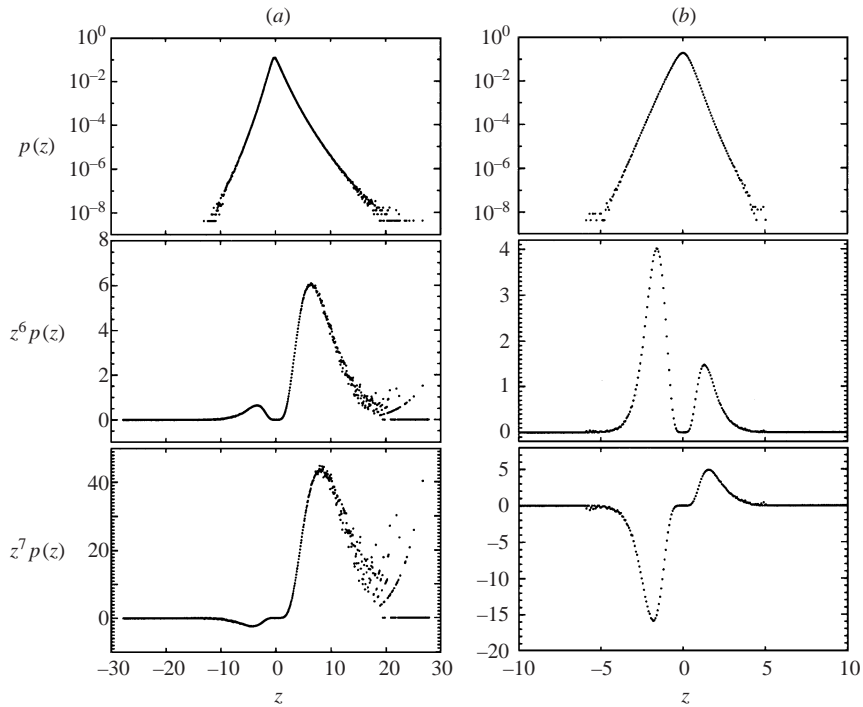

FIGURE 5. Statistical convergence of higher-order derivative moments. (*a*) Results for the normalized transverse derivative, probability density function $p(z)$, $z^6 p(z)$ and $z^7 p(z)$. (*b*) The same functions for the normalized longitudinal derivative. Both data sets are for $R_\lambda = 95$ (run 4).

(1996) for $S_3(\partial u'_x/\partial y)$ and with the experimental data of Shen & Warhaft (2000) at $R_\lambda \sim 100$. The error bars for our data display the standard deviation of the *y* profiles of the moments. Averaging was always performed in time and in planes at fixed *y*. Data points closest to the boundaries are excluded from the evaluation of

the averages. The snapshots of the full velocity field were always separated by at least one shear time unit, $St = 1$. The minimal number of snapshots used was 114 (for run 5). The results are in agreement with previous numerical and experimental findings.

The fluctuations around the mean grow for increasing order as expected; they were subjected to a more detailed investigation. Figure 5 shows the probability density functions (p.d.f.), denoted $p(z)$, of $z = (\partial u'_x/\partial y)/\langle(\partial u'_x/\partial y)^2\rangle^{1/2}$ in column (*a*) and of $z = (\partial u'_x/\partial x)/\langle(\partial u'_x/\partial x)^2\rangle^{1/2}$ in column (*b*). The results are calculated from 6×10^8 data points at $R_\lambda = 95$. A check of the statistical convergence of the nth-order moments can be made by plotting the integrands $z^n p(z)$ over z which is also shown in figure 5. While the longitudinal derivative has converged well, the integrands for the transverse derivative show a strong scatter in the tails of the p.d.f. The area that covers the scattered data measures the uncertainty around the mean in an alternative way.

In the following, we wish to discuss the strong scattering of higher-order moments and will demonstrate by means of a simple analytical model that this is a more general feature for data analysis. The p.d.f. (see figure 5) can be roughly approximated by the normalized exponential distribution $p(z) = (\alpha \cosh(\alpha z_0)/2) \exp(-\alpha|z - z_0|)$ for which all moments can be evaluated analytically, to $\langle z^n \rangle \sim n!$. Let N be the number of statistically independent samples. The standard deviation, which is defined as $\sigma(z^n) = [(\langle z^{2n}\rangle - \langle z^n\rangle^2)/(N-1)]^{1/2}$, follows then as

$$\sigma(z^n) \simeq \pm\frac{1}{\alpha^n}\left[\frac{(2n)! - (\tanh(\alpha z_0)n!)^2}{N}\right]^{1/2}, \tag{4.1}$$

for the odd normalized moments $S_n = \int z^n p(z)\mathrm{d}z$. The denominator was simplified because $N \gg 1$. When taking, e.g. $\alpha = 1$ and $z_0 = 1$, the standard deviation for the seventh moment decreases from 24% at $N = 10^5$ to 1% at $N = 10^8$. Thus, the calculation demonstrates clearly the sensitivity of higher-order moments to N which can give rise to very large fluctuations around the mean as observed in our simulations. While the moment itself is proportional to the factorial of the order, $n!$, its fluctuations become proportional to $((2n)!)^{1/2}$. Tennekes & Lumley (1972) estimated $N(1) = T/(2\tau)$ for a first-order moment, where τ is the integral time scale and T the duration of the measurement. Starting from this point, Sreenivasan, Chambers & Antonia (1978) extracted relations for the accuracy of higher-order moments using their atmospheric boundary layer data. Following their work, the number of statistically independent samples for an nth moment, $N(n)$, would result in $N(n)/N(1) = (0.82 - 0.07\,n)^{-1}$. Aside from the fact that the fluctuations for fixed N and growing n can increase rapidly, this dependence would improve the statistical convergence weakly.

In summary, we have presented an alternative method of modelling a statistically stationary homogeneous shear flow by using stress-free boundary conditions in the y-direction. At the level of second-order moments our results are not in conflict with the classical concepts of local isotropy as indicated by the power spectra of the velocity correlations. We found non-decreasing derivative moments for the orders 4 to 7 which agree with the experimental findings of Shen & Warhaft for $R_\lambda \sim 100$ but are in apparent violation of local isotropy. A next step would be to relate typical structures of turbulent shear flows, such as streamwise vortices and streamwise streaks, to the statistical properties presented here.

REFERENCES

CAUGHEY, S. J., WYNGAARD, J. C. & KAIMAL, J. C. 1979 Turbulence in the evolving stable boundary layer. *J. Atmos. Sci.* **36**, 1041–1052.

FALKOVICH, G. 1994 Bottleneck phenomenon in developed turbulence. *Phys. Fluids* **6**, 1411–1414.

FERCHICHI, M. & TAVOULARIS, S. 2000 Reynolds number effects on the fine structure of uniformly sheared turbulence. *Phys. Fluids* **12**, 2942–2953.

GARG, S. & WARHAFT, Z. 1998 On small scale statistics in a simple shear flow. *Phys. Fluids* **10**, 662–673.

GERZ, T., SCHUMANN, U. & ELGOBASHI, S. E. 1989 Direct numerical simulations of stratified homogeneous turbulent shear flows. *J. Fluid Mech.* **200**, 563–594.

GUALTIERI, P., CASCIOLA, C. M., BENZI, R., AMATI, G. & PIVA, R. 2000 Scaling laws and intermittency in homogenous shear flow. Preprint nlin.CD/0011040; *Phys. Fluids* (submitted).

HAIRER, E., NØRSETT, S. P. & WANNER, G. 1993 *Solving Ordinary Differential Equations I – Nonstiff Problems.* Springer.

LUMLEY, J. L. 1967 Similarity and the turbulent energy spectrum. *Phys. Fluids* **10**, 855–858.

KOLMOGOROV, A. N. 1941 The local structure of turbulence in incompressible viscous fluid for very large Reynolds numbers. *Dokl. Akad. Nauk SSSR* **30**, 301–310.

KURIEN, S. & SREENIVASAN, K. R. 2000 Anisotropic scaling contributions to high-order structure functions in high-Reynolds-number turbulence. *Phys. Rev. E* **62**, 2206–2212.

POPE, S. B. 2000 *Turbulent Flows.* Cambridge University Press.

PUMIR, A. 1996 Turbulence in homogeneous shear flows. *Phys. Fluids* **8**, 3112–3127.

ROGALLO, R. S. 1981 Numerical experiments in homogeneous turbulence. *NASA Tech. Mem.* 81835.

ROGERS, M. M. & MOIN, P. 1987 The structure of the vorticity field in homogeneous turbulent flows *J. Fluid Mech.* **176**, 33–66.

SADDOUGHI, S. G. & VEERAVALLI, S. V. 1994 Local isotropy in turbulent boundary layers at high Reynolds numbers. *J. Fluid Mech.* **268**, 333–372.

SCHUMACHER, J. & ECKHARDT, B. 2000 On statistically stationary homogeneous shear turbulence. *Europhys. Lett.* **52**, 627–632.

SCHUMACHER, J. & ECKHARDT, B. 2001 Evolution of turbulent spots in a parallel shear flow. *Phys. Rev. E* **63**, 046307-1–046307-9.

SHE, Z., CHEN, S., DOOLEN, G., KRAICHNAN, R. H. & ORSZAG, S. A. 1993 Reynolds number dependence of isotropic Navier-Stokes turbulence. *Phys. Rev. Lett.* **70**, 3251–3254.

SHEN, X. & WARHAFT, Z. 2000 The anisotropy of the small scale structure in high Reynolds number ($R_\lambda \sim 1000$) turbulent shear flow. *Phys. Fluids* **12**, 2976–2989.

SREENIVASAN, K. R. 1998 An update on the energy dissipation rate in isotropic turbulence. *Phys. Fluids* **10**, 528–529.

SREENIVASAN, K. R., CHAMBERS, A. J. & ANTONIA, R. A. 1978 Accuracy of moments of velocity and scalar fluctuations in the atmospheric surface layer. *Boundary-Layer Met.* **14**, 341–359.

TENNEKES, H. & LUMLEY, J. L. 1972 *A First Course in Turbulence.* The MIT Press.